Low Ion Velocity Stopping in Binary Ionic Mixtures and Strongly Coupled H-He Plasmas

C. DEUTSCH[1], B. TASHEV[2], P. FROMY[1] and R. POPOFF[1]

1-LPGP, UPS Orsay, Fr
2. Dpt Physics, Almaty, Kz

EMMI GSI-IHED Workshop, MAI 2-4 2011

The basic LIVSD behavior is, as well-known of the form

$$-\frac{dE}{dx} = Av_p$$

in the low ion projectile velocity limit advocated previously with energy/nucleon E/A ≤ 100 keV/amu.

Within the dielectric framework of present concern, we consider the electromagnetic response of a target plasma built on electrons and ion species (Z_i, M_i). The target ion part is taken here as a weakly coupled binary ionic mixture (BIM), which will prove sufficient in the subsequent considered plasma targets. In such an approach, it appears useful to work wtih the overall dielectric function

$$\varepsilon(\vec{k},\omega) = 1 + \frac{1}{k^2}\left(W\left(\frac{W}{k}\right) + W\left(\sqrt{M_1}\frac{W}{k}\right) + W\left(\sqrt{M_2}\frac{W}{k}\right)\right)$$

with the usual Fried-Conte dispersion function W(Im$\zeta \geq 0$)

$$W(\varsigma) = \frac{1}{\sqrt{2\pi}} \lim_{\nu \to 0+} \int_{-\infty}^{\infty} dx \frac{x e^{-x^2/2}}{x - \varsigma - i\nu}$$

and $X(\zeta)=\mathrm{Re}W(\zeta)$, $Y(z)=\mathrm{Im}W(\zeta)$.

Cf P. Fromy, B. Tashev and C Deutsch. PRSTAB **13**, 101302 (2010) and EPL **92**, 15002 (2010)

Generalizing the standard one-component stopping quadrature

$$-\left[\frac{dE}{dx}\right]=\frac{Z^2 N_D}{(2\pi)^2}\int_0^{k_{max}} dk\ k^3 \int_{-1}^{+1} d\mu \frac{\mu Y(\mu v_p)}{\left[k^2+X(\mu v_p)\right]^2+Y^2(\mu v_p)}$$

with $Z = Z_{eff}/N_D$, where Z_{eff} denotes the projectile effective charge at velocity v_p, $N_D=n_e\lambda^3_{De}$ in terms of target electron density and corresponding Debye length. In the sequel, v_p will be scaled by , thermal electron velocity with T, thermalized target temperature.

$$k_{max}=\mathrm{Min}\left(\frac{m(v_p^2+v_{the}^2)}{Z_{eff}\ e^2},\ \frac{2m\sqrt{v_p^2+v_{the}^2}}{\hbar}\right)$$

$$=\mathrm{Min}\left(\frac{4\pi}{Z}(v_p^2+2),\ 8\pi\sqrt{2N_D}\frac{\alpha c}{v_{the}}\sqrt{v_p^2+2}\right)$$

Where v_p is now dimensionless on the second line on the right-hand-side. α=1/137 is the fine structure constant, and c, light velocity.

In adapting to BIM stopping, it proves convenient to introduce the relative ion concentration of species 1, i.e

$$\alpha = \frac{N_1}{N_1 + N_2}$$

in terms of ion number N_i with i = 1,2, in target plasma, so that BIM densities

$$n_1 = \frac{n_e \alpha}{\bar{Z}}, \quad n_2 = \frac{n_e (1-\alpha)}{\bar{Z}}, \quad \bar{Z} = Z_1 \alpha + Z_2 (1-\alpha)$$

are straightforwardly expressed in terms of electron density n_e.

Then, we can estimate the stopping contributions of every target component : electron (0), ion 1 and ion 2 as follows

$$-\frac{dE_0}{dx} = C_0 \int_0^{k_{max0}} dk\ k^3 \int_{-1}^{+1} d\mu \frac{\mu Y[\mu v]}{D[k, \mu v]}$$

$$-\frac{dE_1}{dx} = C_1 \int_0^{k_{max1}} dk\ k^3 \int_{-1}^{+1} d\mu \frac{\mu Y\left[\sqrt{M_1}\, \mu v\right]}{D[k, \mu v]}$$

$$-\frac{dE_2}{dx} = C_2 \int_0^{k_{max2}} dk\ k^3 \int_{-1}^{+1} d\mu \frac{\mu Y\left[\sqrt{M_2}\, \mu v\right]}{D[k, \mu v]}$$

where

$$D\left[k,\ \mu v_p\right] = \left(k^2 + X\left[\mu_p v_p\right] + X\left[\sqrt{M_1}\mu v_p\right] + X\left[\sqrt{M_2}\mu v_p\right]\right)^2 \quad ,$$

$$+\left(Y\left[\mu v_p\right] + Y\left[\sqrt{M_1}\mu v_p\right] + Y\left[\sqrt{M_2}\mu v_p\right]\right)^2 \quad , \tag{8}$$

$$C_0 = \frac{k_B T\ Z_{eff}^2}{4\pi^2 n_e \lambda_{D_e}^4} \quad , \tag{9a}$$

$$C_1 = \frac{C_0 Z_1^2 \alpha}{\overline{Z}} \quad , \tag{9b}$$

$$C_2 = \frac{C_0 Z_2^2 (1-\alpha)}{\overline{Z}} \quad , \tag{9c}$$

altogether with

$$k_{max_0} = \mathrm{Min}\left(k_{max_0^1} = n_e \lambda_{D_e}^3 \frac{4\pi(v^2+2)}{Z_{eff}},\ 185.73\ n_e \lambda_{D_e}^3 \sqrt{\frac{v^2+2}{T(eV)}}\right), \tag{10a}$$

$$k_{max_1} = \frac{k_{max_0^1}}{Z_1^3} \left(\frac{\overline{Z}}{\alpha}\right)^{1/2} , \tag{10b}$$

$$k_{max_2} = \frac{k_{max_0^1}}{Z_2^3} \left(\frac{\overline{Z}}{1-\alpha}\right)^{1/2} . \tag{10c}$$

Expressions (7a-7c) are in k_{BT}/λ_D, with the Debye screening length λ_D respectively adapted to electron, ion 1 and ion 2. v_p is in $v_{the.}$

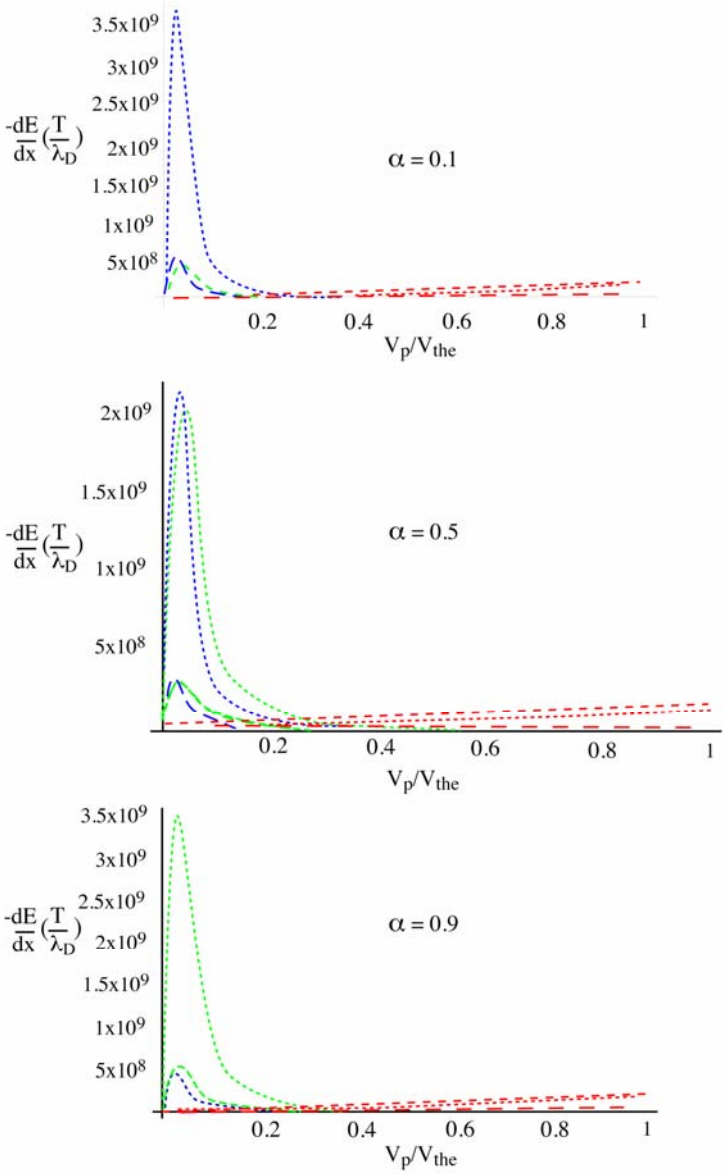

Figs. 1 - Proton stopping in H^+-D^+ BIM in terms of v_p/v_{the}.
$n_e = 10^{23}$ e-cm^{-3} alpha denotes proton concentration in BIM
T(eV) = ····· 10, - - - - - 100, – – – 1000.
Red pertains to e-stopping, green to H^+-stopping
and blue to D^+-stopping.

In the sequel α denotes the relative proportion of ion species A in the AB-BIM. As a prerequisite to this program, we detail on Figs. 1 the α-dependence of the stopping profiles (SP) in terms of dimensionless projectile velocity v_p/v_{the} for proton projectiles losing their energy in a H^+-D^+BIM at solid density $n_e=10^{23}$ e-cm^{-3} and T(eV)=10-1000, BIM stopping appear mostly restricted to the narrow range $0 \leq v_p/v_{the} \leq 0.2$.

It is also a remarkable fact that the target ion SP peaks always lie at very low $v_p/v_{the} \leq 0.05$, on the three cases (Figs. 1-3) up to now considered.

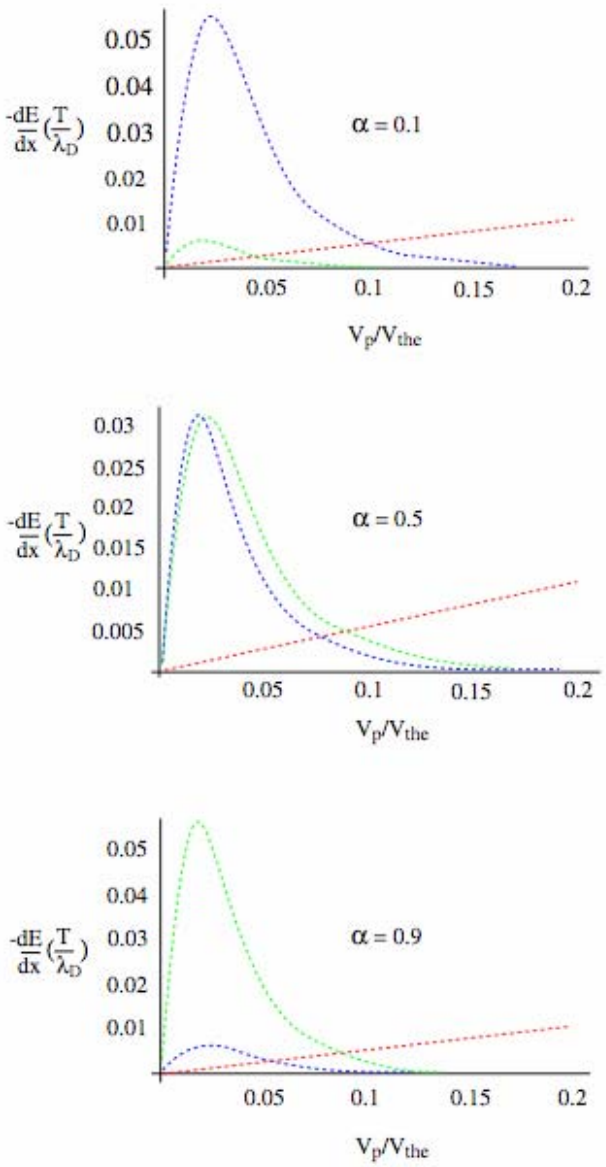

Figs. 2 - Alpha particle stopping in a Tokamak-like D-T BIM with $n_e = 10^{14}$ e-cm^{-3} and T =10 keV. α denotes D^+-concentration. Red refers to e-stopping, green to D^+-stopping and blue to T^+-stopping.

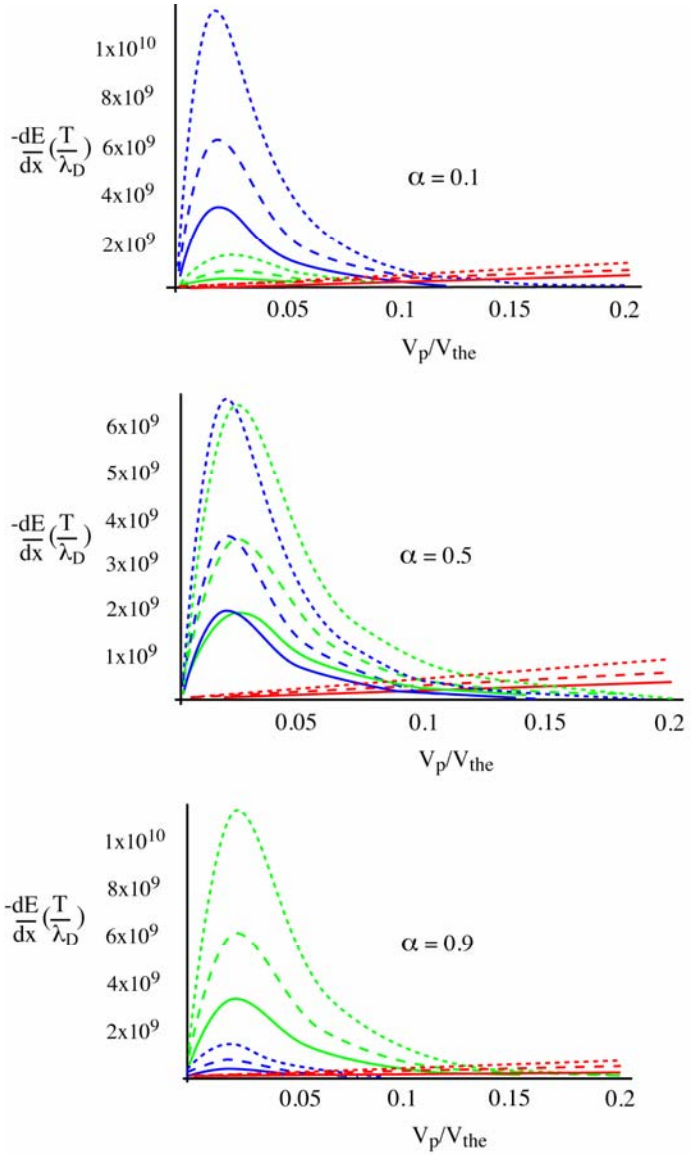

Figs. 3 - Proton stopping in a DT-mixture. $n_e = 10^{25}$ e-cm^{-3}
T(eV) = ····· 500, - - - - - 1000, —— 2000.
Red refers to e-stopping, green to D^+-stopping
and blue to T^+-stopping. α = D^+-concentration.

T-dependence

In view of the crucial dependence of FIS ignition performances on the initial temperature of the compressed DT-fuel we detail on Figs. 4-5 stopping profiles (SP) on a logarithmic scale for alpha particle slowing down at 10^{23} e-cm^{-3} and 10^{26} e-cm^{-3}, respectively. With this change of scale, the e-stopping does not appear negligible and the fine structures at the intersection of electron SP and ions SP are clearly shown. α denotes deuterium relative concentration and the quasi-symmetric features of target ions SP appear even enhanced contrasted to their linear counterparts.

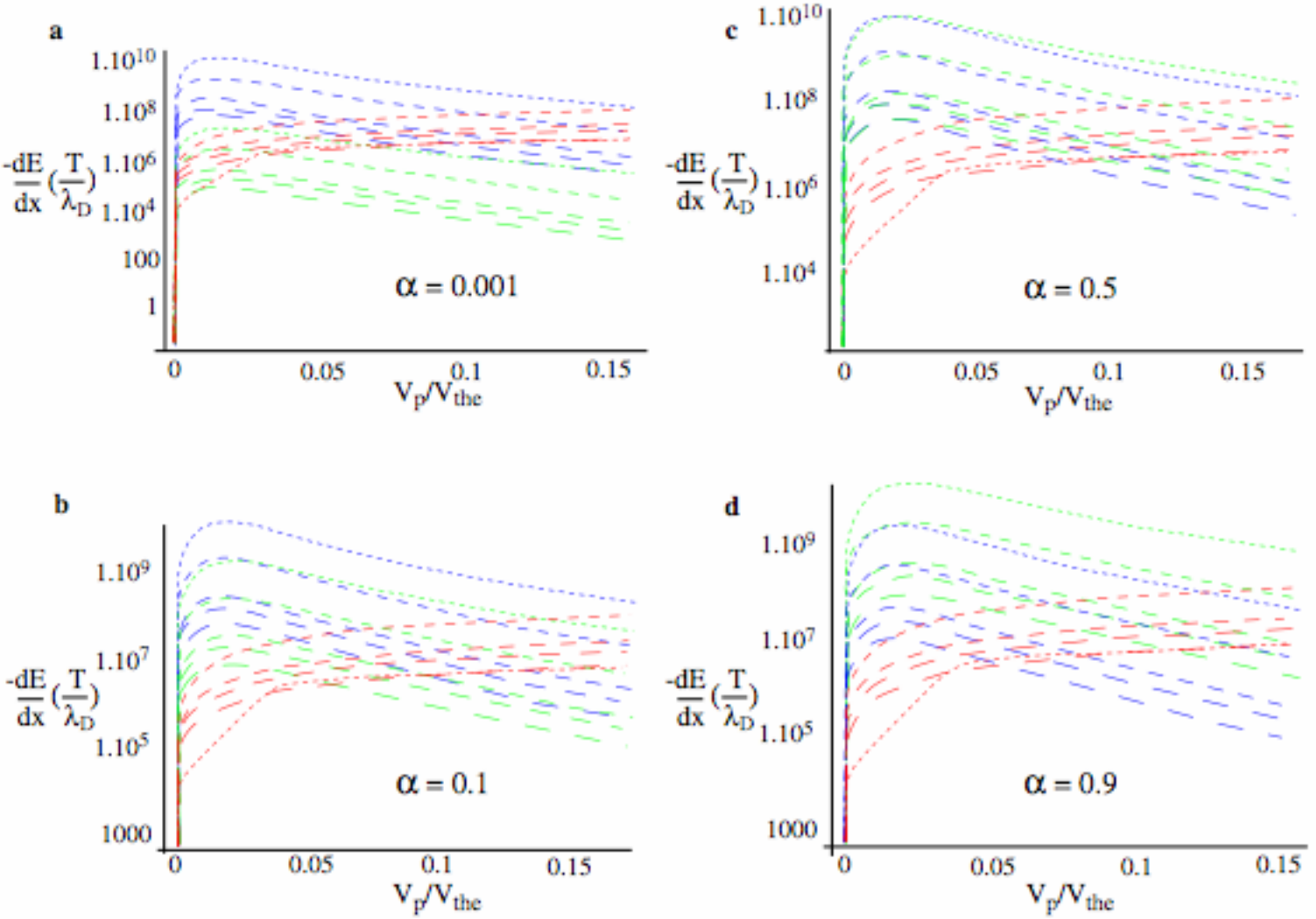

Figs. 4 - Alpha particle projectile in a Deuterium-Tritium BIM with $n_e = 10^{23}$ e-cm^{-3} and temperatures = ····· 10 eV, - - - - - 100 eV, — — — — 1 keV, — — — — 2 keV, — — — 5 KeV with D^+ relative proportion **a)** $\alpha = 0.001$, **b)** $\alpha = 0.1$, **c)** $\alpha = 0.5$ and **d)** $\alpha = 0.9$. Red refers to electron stopping, green to D^+-stopping while blue denotes T^+-stopping, $-dE/dx\ (T/\lambda_D)$ in terms of v_p/v_{the}.

Fig. 6a highlights a rather flat three-dimensional snapshot for a $\alpha = 0.5$ BIM confirming $0.1 \leq v_{p,crit}/v_{the} \leq 0.13$. However separate variations in T (Figs. 6b) and density (Fig. 6c) document a strong α-dependence for $v_{p,crit}$. It is highly suggestive that these $v_{p,crit}$ estimates fall in quite a close agreement with those derived from an independent Fokker-Planck analysis based on ratio of projectile kinetic energy to that of target electrons. So, we have

$$\frac{\frac{1}{2} M_p \, v_{p,crit}^2}{\frac{1}{2} m_e \, v_{the}^2} = \frac{C^{2/3}}{\frac{1}{2} m_e \, V_{the}^2}$$

where

$$C = \frac{3 \, \pi^{1/2}}{4} \left(\frac{M_p}{m_e}\right)^{1/2} \cdot \frac{M_p}{\overline{M}} \cdot \overline{Z}$$

in terms of the BIM quantities $\overline{Z} = \alpha Z_1 + (1-\alpha) Z_2$ and $\overline{M} = \alpha M_1 + (1-\alpha) M_2$.

In the presently considered case, the above ratio yields

$$\frac{v_{p,crit}}{v_{the}} \cong 0.12$$

in a rather good agreement to that given on Fig.6a vertical scale. A similar quantitative matching between present dielectric approach and collision one a la Fokker-Planck of current use in Tokamak physics can be obtained for alpha particle stopping, as well.

Critical velocity $v_{p,crit}$

From all the above displayed numerical patterns, it obviously transpires that the electronic contribution to projectile ion stopping matches the sum of the target ions contributions for a critical projectile velocity $v_{p,crit}$ such that $v_{p,crit}/v_{the}$ ~ 0.15-0.2, provided the given BIM are not too asymmetric in charge and mass.

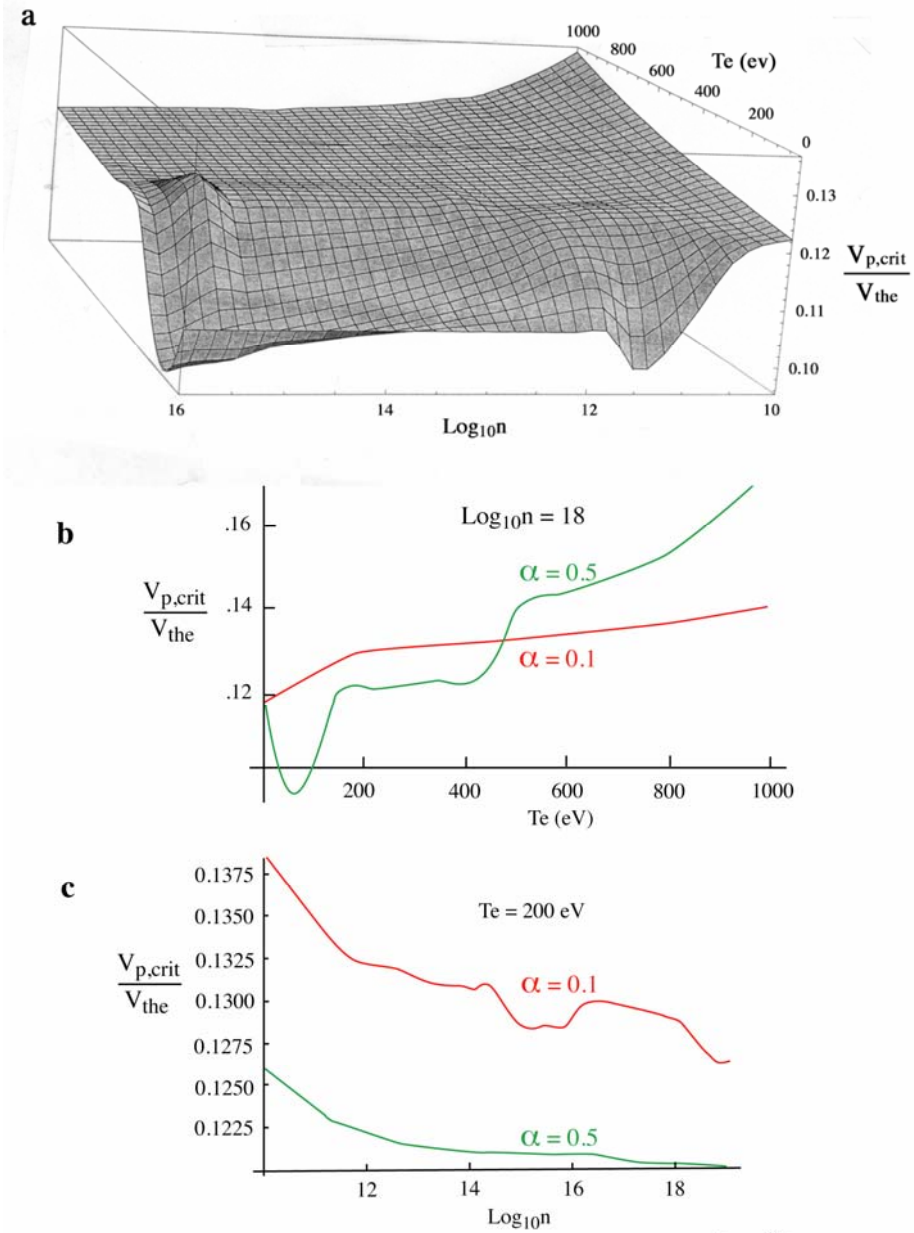

Figs. 6 - Critical proton velocity $v_{p,crit}$ in a $\alpha = 0.5$ H^{+}-He^{2+} BIM

a) 3D view in terms of n_e and T,

b) cross-section at $n_e=10^{18}$ e-cm^{-3} for $\alpha = 0$ and 0.5,

c) cross-section at T =200 eV for $\alpha = 0.1$ and 0.5.

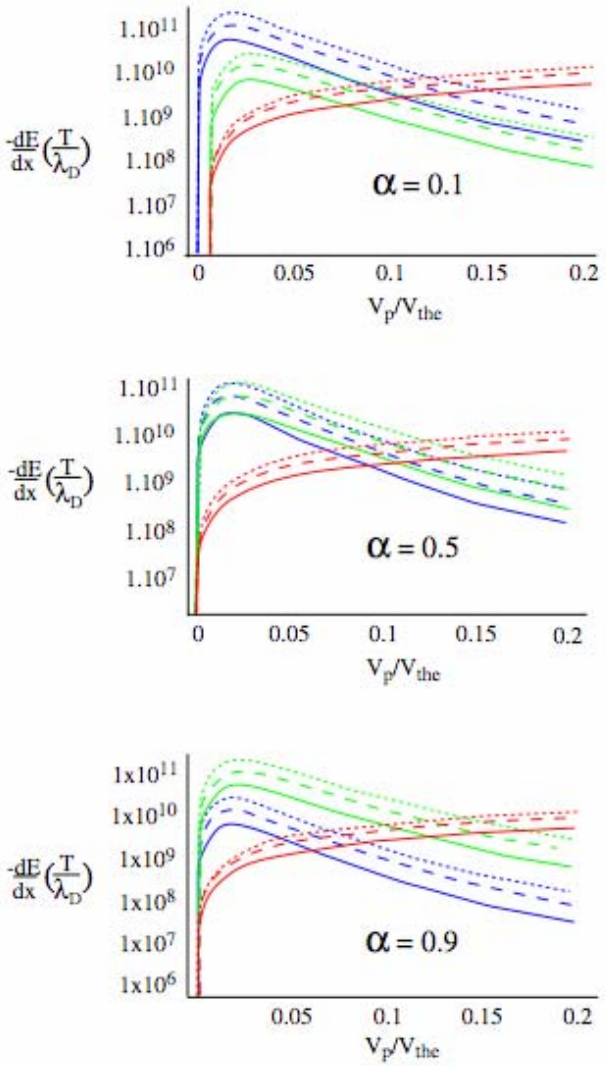

Figs. 5- He^{2+} projectile in a deuterium-tritium mixture where $n_e = 10^{26}$ e-cm^{-3} and
T(keV) = ····· 1, – – – – – 2, ——— 5
with α deuterium relative concentration.
Color attributions are as on Figs 4.

Straggling

In the present high temperature range of interest, the statistical properties of our LIVSD approach essentially rely on the high-T straggling approximation

$$\Omega^2 = 2k_B TS$$

where S is the total stopping including electron and ions contributions. Fig.7 displays the case of proton projectiles stopped in a DT-equimixture (a = 0.5) with n_e (cm^{-3}) = 10^{18} and T(eV) = 500. It unambiguously contrasts the usual bell-shaped curve featuring e-stopping at any v_p, to the highly spiked BIM contribution restricted to $v_p/v_{the} \leq 0.2$.

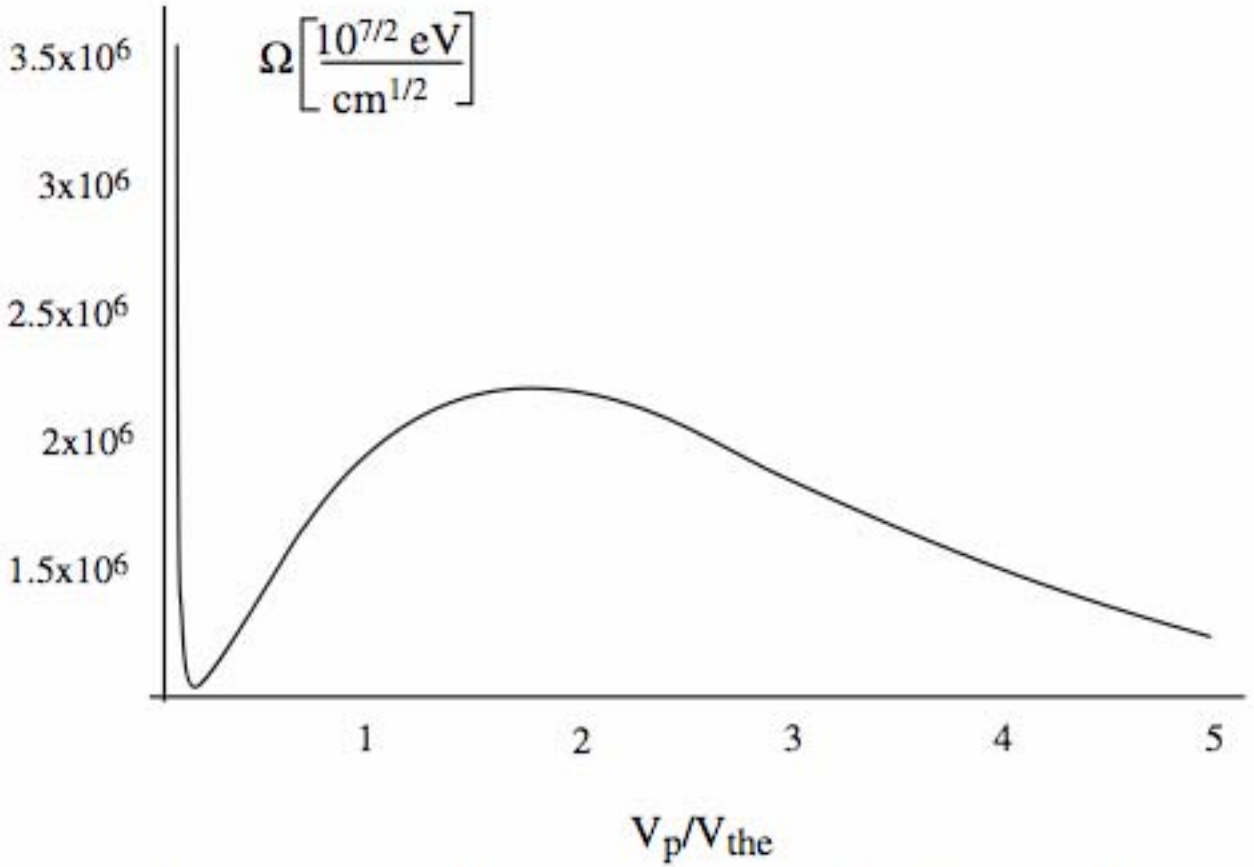

Fig. 7- High temperature straggling for proton projectiles in a DT-BIM with $\alpha = 0.5$, $n_e = 10^{19}$ e-cm^{-3} and T = 500 eV.

ASYMMETRIC BIM

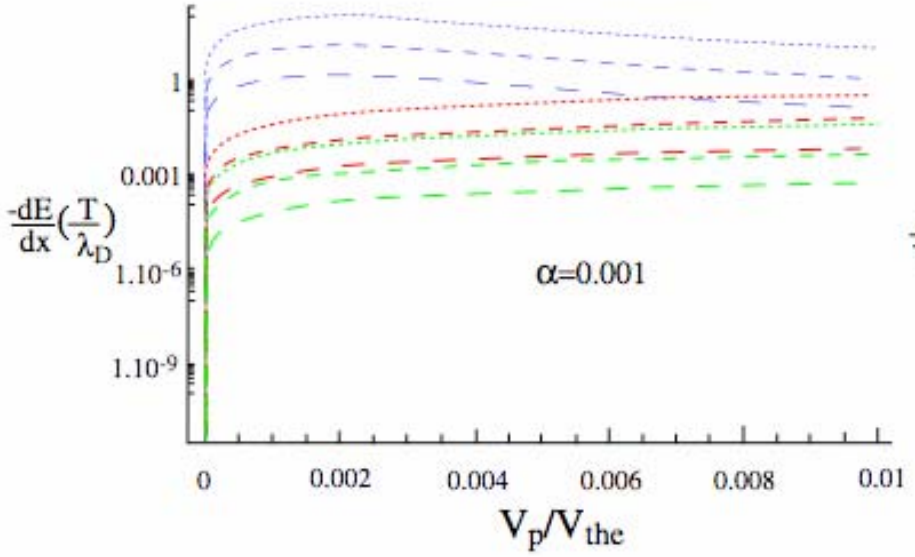

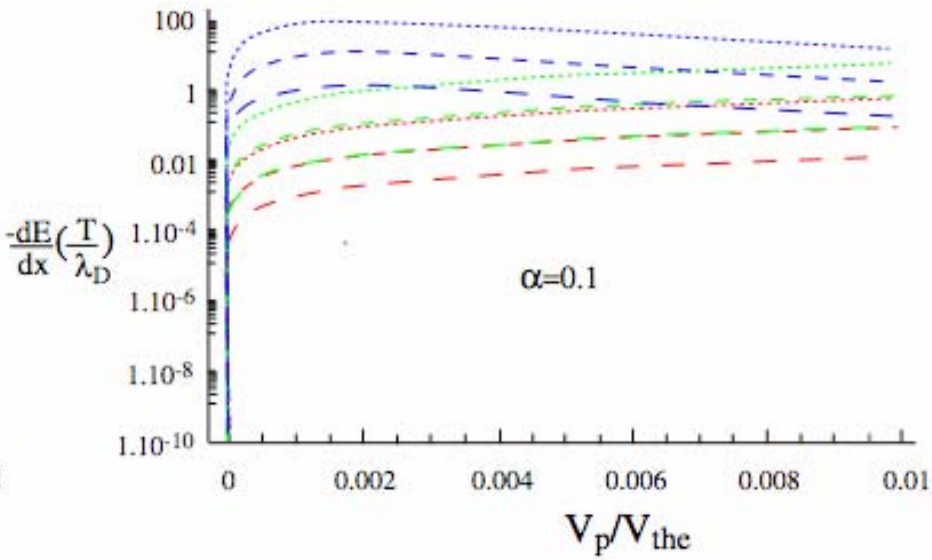

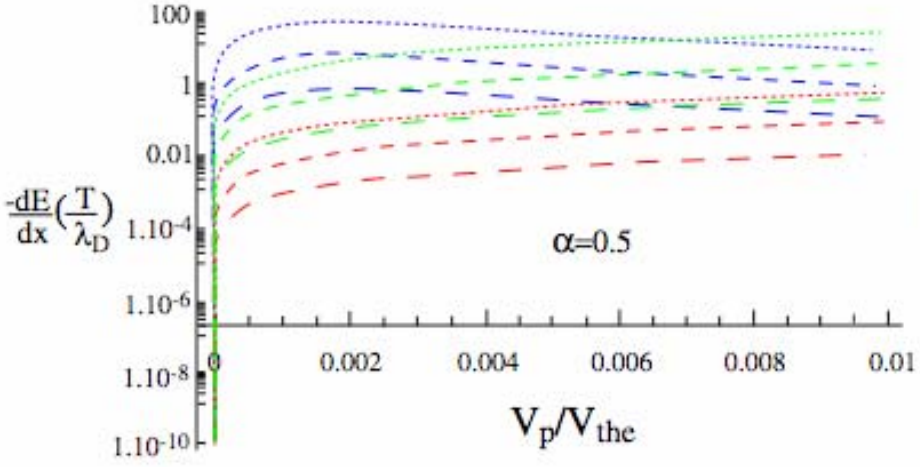

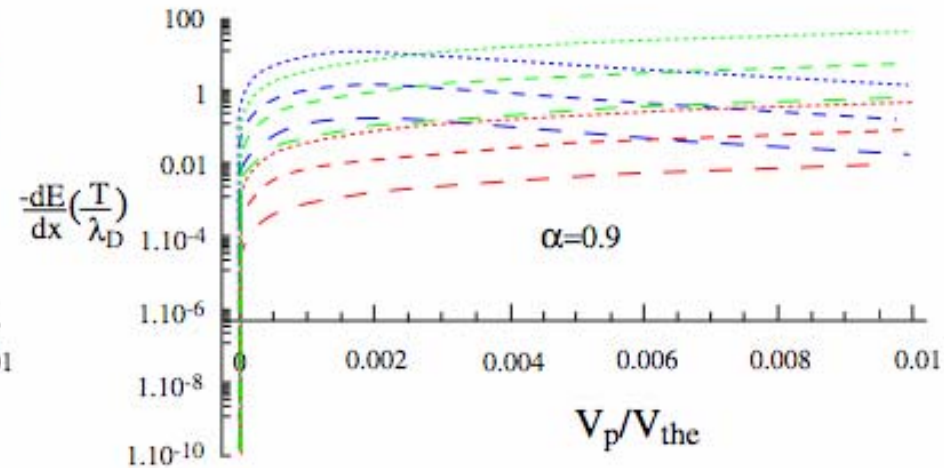

Proton stopping in (proton, U^{+}_{238}) mixture $n_e=10^{14}$ e-cm^{-3}. T(eV)= ····· 1, - - - - - - 10, — — — — 100
Red (e^--stopping), Green (H^+-stopping) and Blue (U^{+}_{238}-stopping)

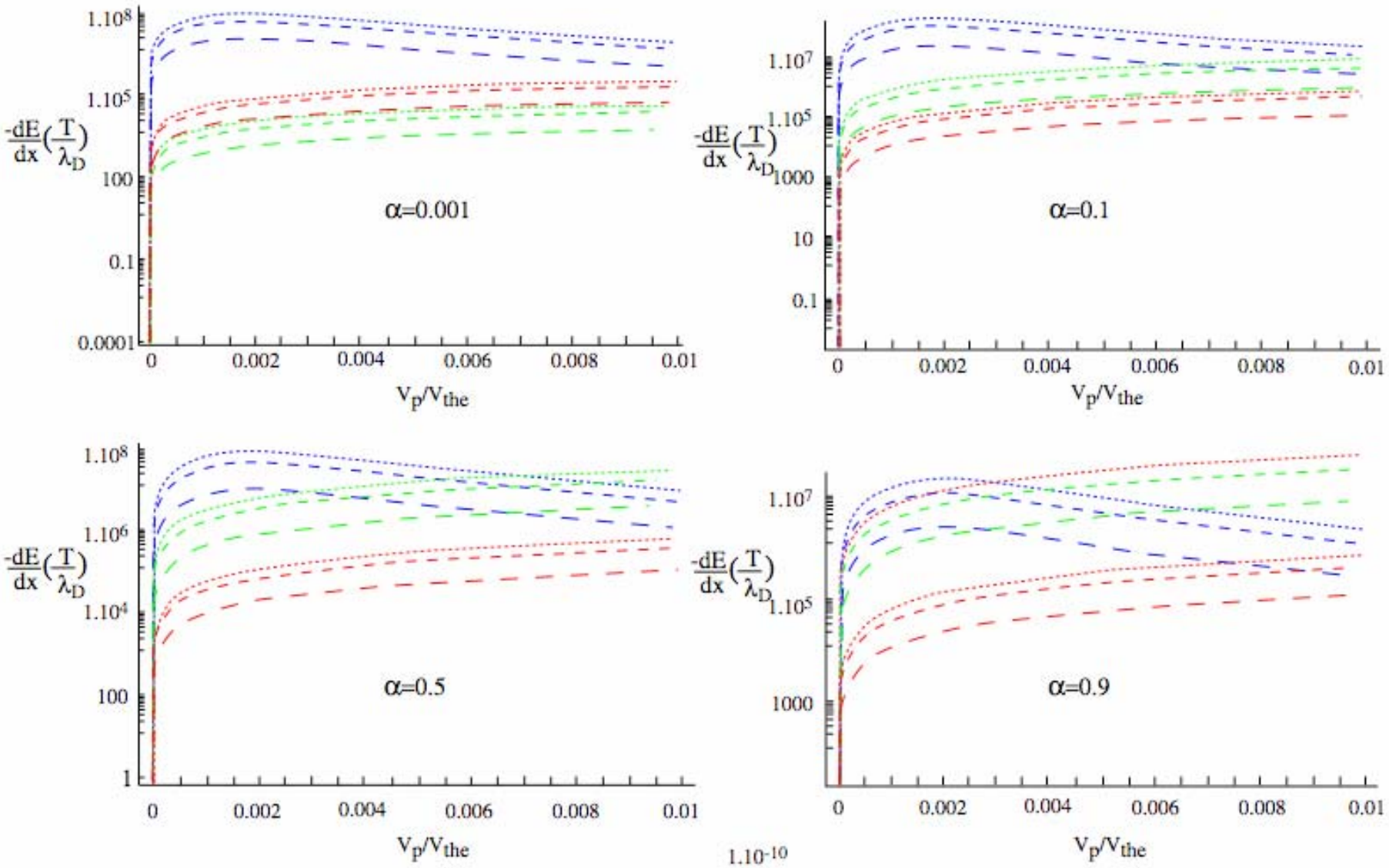

Proton stopping in (proton, U^{+}_{238}) mixture $n_e=10^{23}$ e-cm^{-3}. T(eV)= ····· 500, - - - - - , 1000 — — — — 5000
Red (e^--stopping), Green (H^+-stopping) and Blue (U^{+}_{238}-stopping)

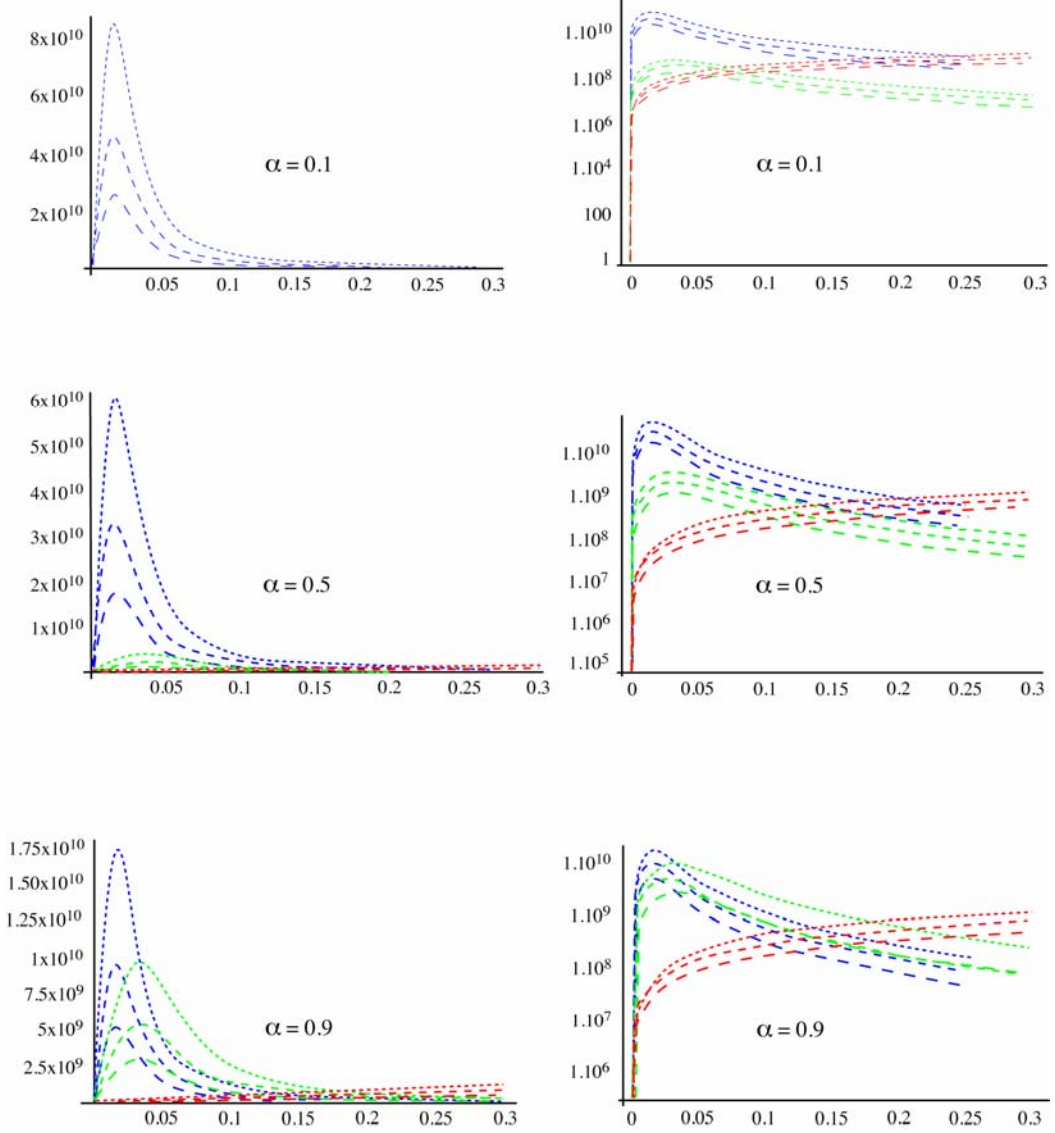

Fig. 8 - Proton slowing down in - dE/dx (T/λ_D) in a H^+-He^{2+} BIM at $n_e = 10^{25}$ e-cm^{-3} and T(eV) = ····· 500, - - - - - - 1000 and - - - - - - 2000,

α qualifies the proton relative proportion.

Red pertains e-stopping, green to H^+-stopping and blue to He^{2+}-stopping.

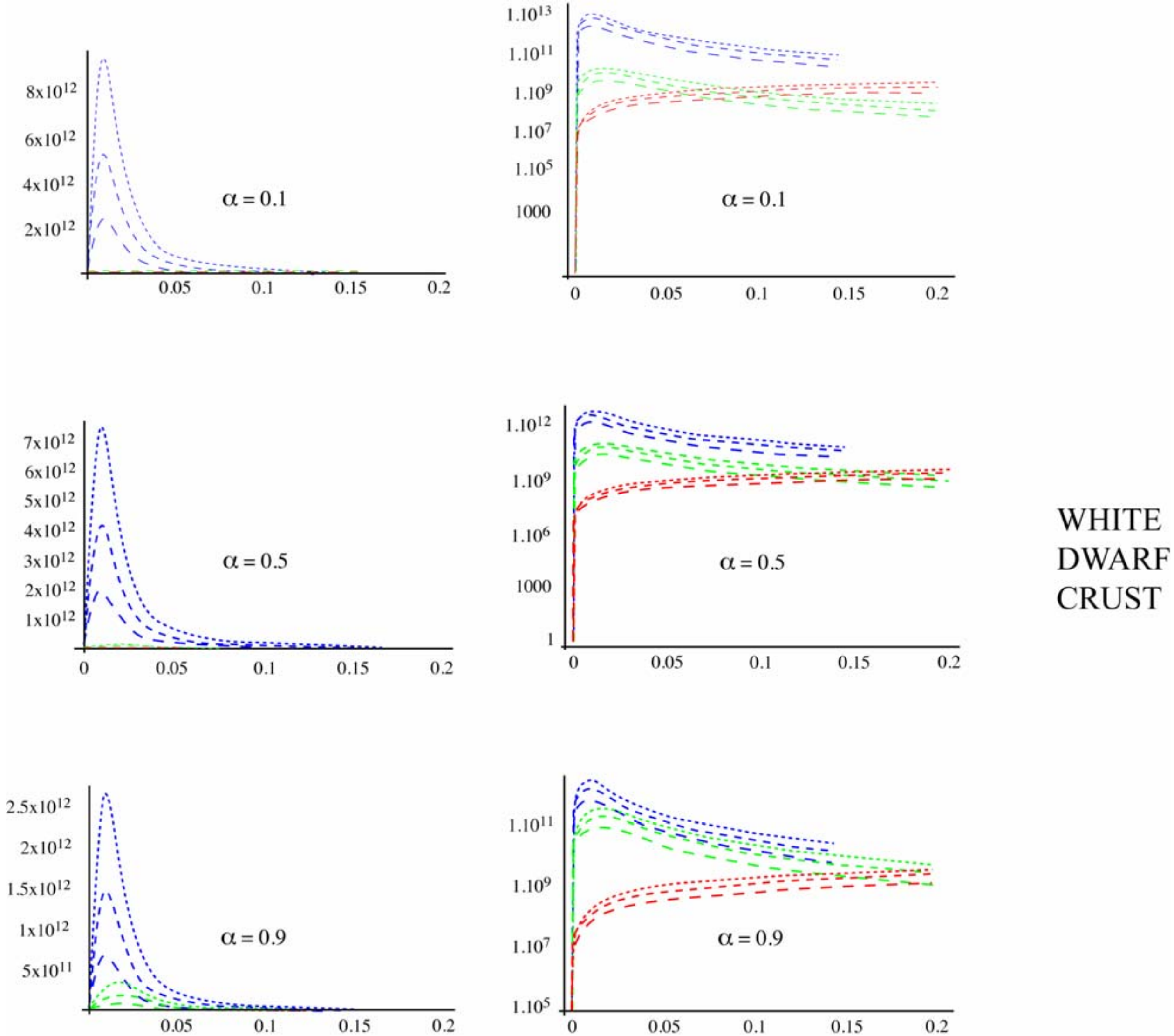

Fig. 10 - Proton - dE/dx (T/λ_D) w.r.t v_p/v_{the} in a He^{2+}-C^{6+} BIM at $n_e = 10^{26}$ e-cm^{-3}

with T(keV) = ... 1, - - - - - - - 2 and — — — — — 5,

α = He^{2+} concentration.

Red denotes e-stopping, green to He^{2+}-stopping and blue to C^{6+}-stopping.

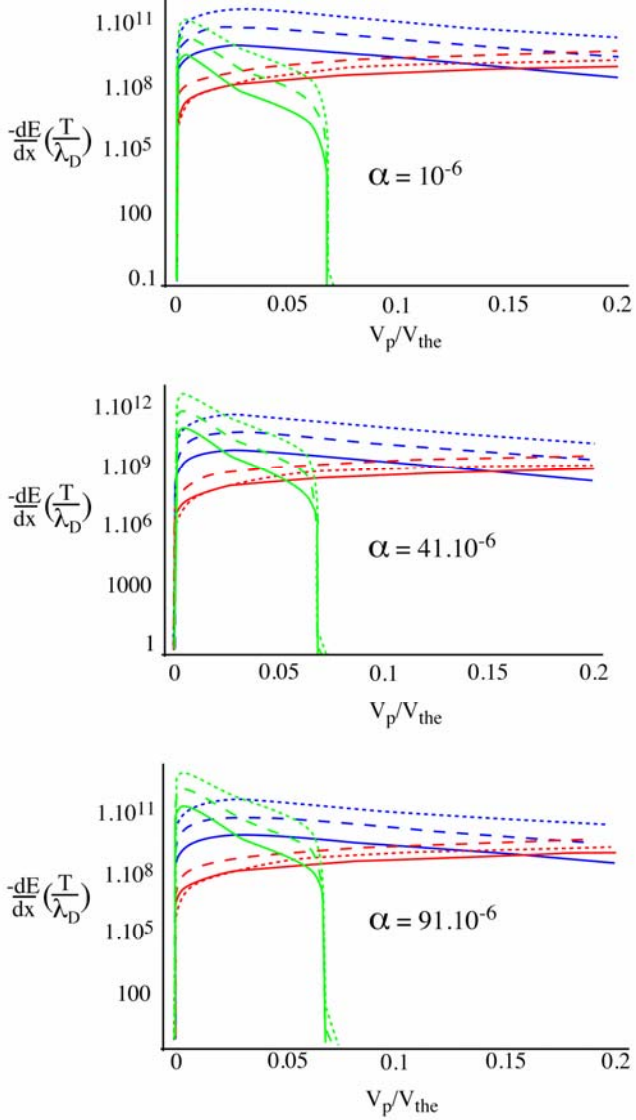

SOLAR INTERIOR

Figs. 11 - Proton projectile in a H^+-Fe^{24+} BIM at $n_e = 10^{26}$ e-cm^{-3}.

T(keV) = ····· 0.1 , - - - - - 1 , ——— 10

With α, relative Fe^{24+} concentration,

a) $\alpha = 10^{-6}$, **b)** $\alpha = 41 \times 10^{-6}$ and **c)** $\alpha = 91 \times 10^{-6}$.

Red denotes e-stopping, green pertains to Fe^{24+}-stopping and blue to H^+-stopping.

Widening the α-scope up to 0.9, we can appreciate the three dimensional landscapes on Figs. 12, including continuous temperature variations on the $0 \leq T(eV) \leq 200$ range at a much lower $n_e=10^{23}$ e-cm^{-3} density, thus possibly featuring the interior of an hypothetical star, yet to be discovered. Here, we can see that for all values of α, now featuring the H^+ relative concentration, the given landscapes differ only for $V_p/V_{the} \leq 0.2$. The low V_p transverse ridge increases with decreasing α. It is the highest at $\alpha = 10^{-3}$, i.e. for a 99.99 Fe^{24+} concentration.

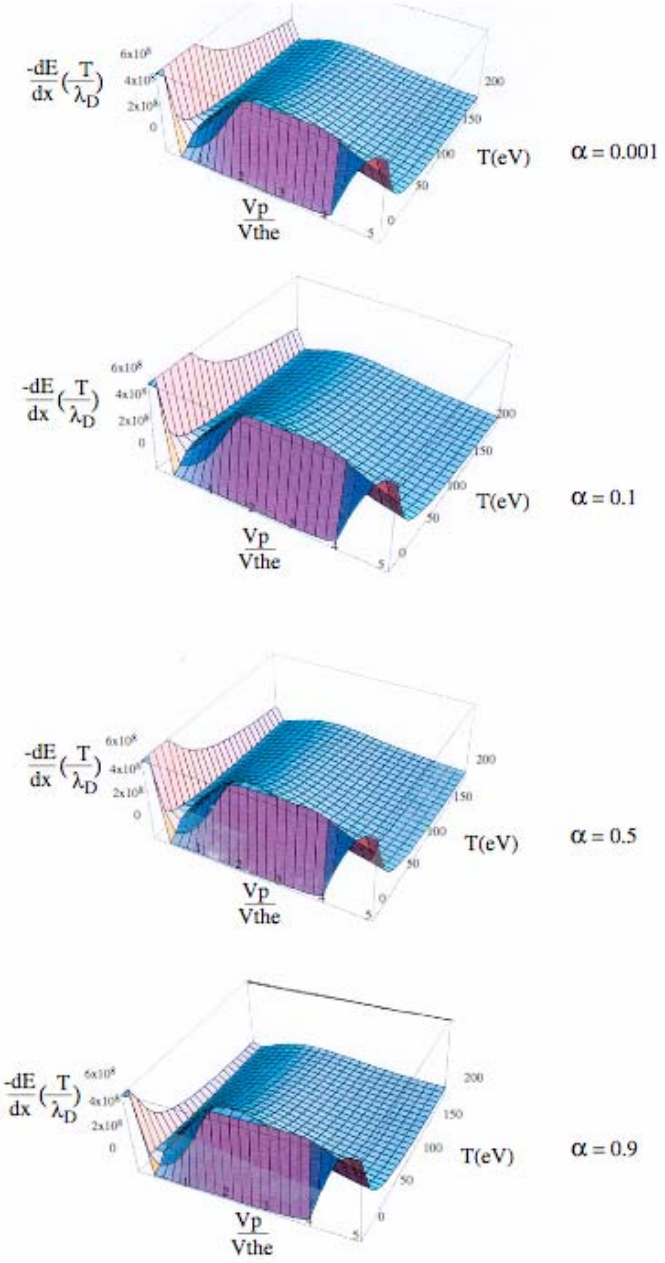

Figs. 12- Proton projectile in H^{+}-Fe^{24+} at $n_e = 10^{23}$ e-cm^{-3} in terms of v_p/v_{the} and T(eV). α denotes H^{+} relative concentration.

Antisymmetric BIM

The present formalism also affords the opportunity to include negatively charged ions in the BIM qualifying the stopping target. Recent low temperature plasma experiments dedicated to the volume production of negatively charged hydrogen ion H^- display the possibility of stopping low energy ions to diagnose quantitatively the BIM properties to which they belong.

With these provisos in mind, we consider on Figs. 13 proton stopping in a H^--H^+ BIM with a rather low total ion density $n_{H-} + n_{H+}$ = 10^11 cm-3 at T(eV) = 0.3, to comply with experiments requests. Considering an overall neutral e-H^--H^+ target plasma, we see on Figs. 13 that the e-stopping contribution gradually decreases with increasing H^- concentration. At $\alpha = 0.5$, the electron fluid has just desappeared as a stopping contributor.

As in previously positively charged BIM, the sum of the two target ion stopping maximua remains constant.

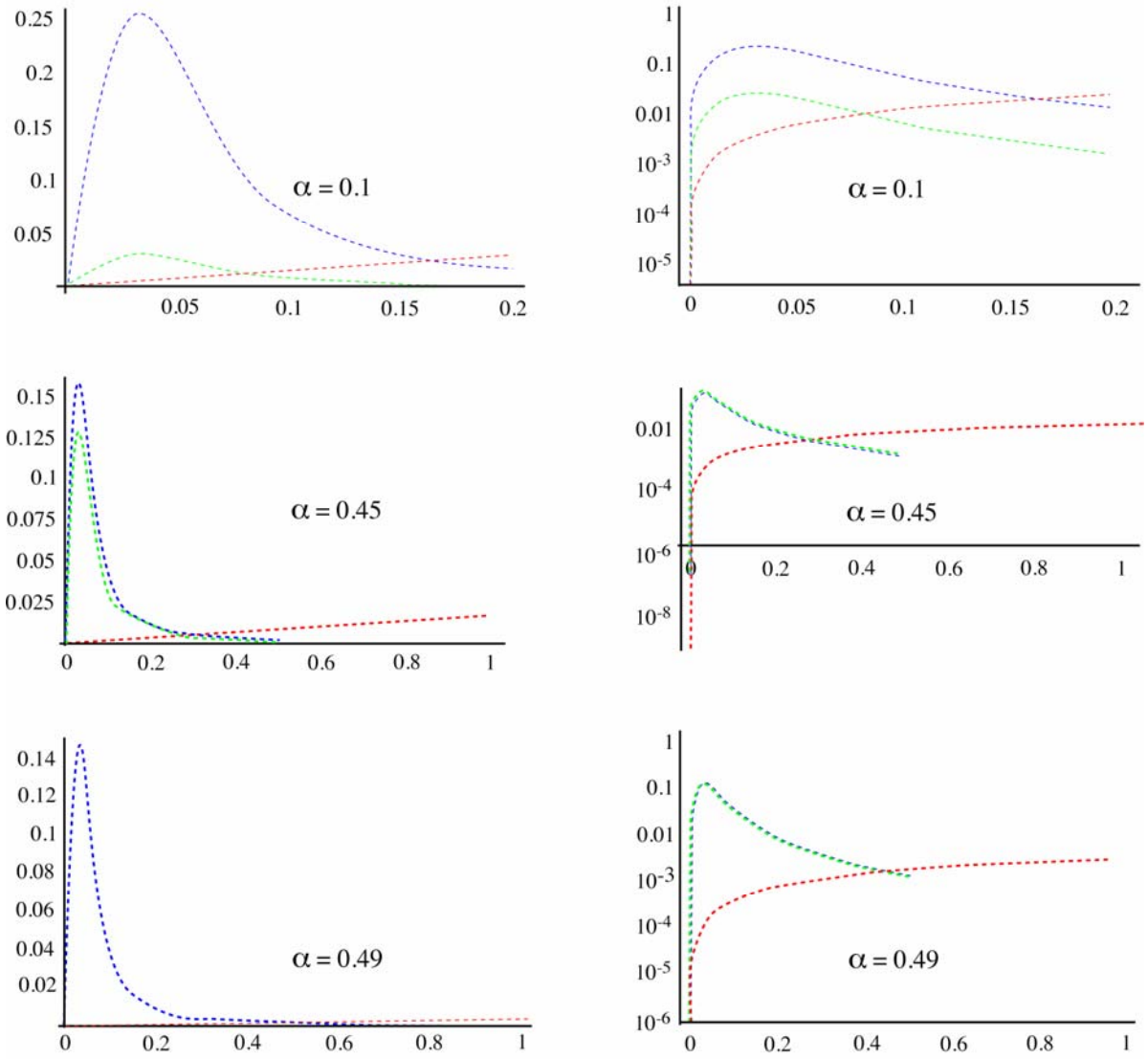

Figs. 13 - Proton - $dE/dx\ (T/\lambda_D)$ in terms of v_p/v_{the} in a H^--H^+ BIM with total ion density = 10^{11} e-cm^{-3}. α denotes H^- relative concentration.

Red refers to e-stopping, green to H^--stopping and blue to H^+-stopping. T(eV) = 0.3.

Low Ion Velocity Slowing Down in a Strongly Coupled and Demixing H-He BIM

Cf C. Deutsch, D. Leger and B. Tashev LPB **29**, 121 (2011)

D. Leger and C. Deutsch, Phys. Rev.A**37**, 4916-4930 (1988)

$$\Gamma_i = \frac{Z_i^2 e^2}{k_B T a_i} \qquad (1)$$

where $a_i = (\frac{4\pi}{3} n_i)^{-1/3}$ with temperature $T=T_e=T_i$. Here we stress strongly coupled BIM with $\Gamma_i >> 1$, able to display a critical demixing process.

A critical demixing behaviour is observed on the ion-ion structure factor $S_{\alpha\beta}(q)$ in the long-wavelength $q \rightarrow 0$ limit.

LVISD is essentially monitored by the projectile interaction with target ions. A foremost motivation for the present undertaking is a possible involment of LVISD in BIM in probing and testing the ion demixtion process. Whitin a dielectric framework for target particles, the nonrelativistic ion stopping thus reads as

$$S = -\frac{dE}{dx} = -\frac{1}{V_p}\left(\frac{dE}{dt}\right)_0 = \frac{2}{\pi}\left(\frac{Z_p e}{V_p}\right)^2 \int_0^\infty \frac{dq}{q} \int_o^{qV_p} d\omega\omega \, Im\left(-\frac{1}{\varepsilon(q,\omega)}\right), \qquad (2)$$

which can be straightforwardly reexpressed in terms of the ion charge-ion charge structure factor when switching to very low

$$V_p \leq \overline{V_{thi}} = C_1 V_{th1} + C_2 V_{th2},$$

with V_{thi}, thermal velocity and C_i, relative concentration of ion i.

In coming ion projectile could then be able to probe every available ion fluid fluctuations in target by restricting the global dielectrics expression $\varepsilon(q,\omega)$ to its i-component. Such a picture highlights the BIM electron background following the ionic fluctuations, within a polarization concept.

Energy exchange between ion projectile and thermalized medium is expressed in terms of emission and absorption processes, according to the protocole (Pines, 1964)

$$\left.\frac{dE}{dt}\right)_0 = \int_{\omega>0} d^3\vec{q} N(\omega) f(\vec{q},\omega) - \int_{\omega>0} d^3\vec{q} (N(\omega)+1) f(\vec{q},\omega)$$

Yielding, up to first order in the interaction, a quadrature involving only spontaneous emission.

$$S_{zz}(\vec{q},\omega) = \frac{\hbar q^2}{4\pi^2 e^2} N(\omega) \mathrm{Im}\left(-\frac{1}{\varepsilon(q,\omega)}\right) \qquad (3)$$

where $N(\omega)^{-1} = e^{\beta\hbar\omega} - 1$, $\beta = (k_B T)^{-1}$ allow to put –dE/dx under the form

$$S = \frac{2}{\pi}\left(\frac{Z_p e}{V_p}\right)^2 \int_0^\infty \frac{dq}{q} \int_o^{qV_p} d\omega \frac{4\pi^2 e^2 \omega}{\hbar q^2} S_{zz}(\vec{q},\omega)\left(e^{\beta\hbar\omega} - 1\right) , \qquad (4),$$

with the usual electron $\varepsilon(q,\omega)$ now extended to the ion components building up the BIM, and the charge-charge structure factor

$$S_{zz}(q) = \sum_{\alpha,\beta=1}^{2} (c_\alpha c_\beta)^{1/2} Z_\alpha Z_\beta S_{\alpha\beta}(q) \ , \qquad (5)$$

where $C_1+C_2 = 1$

Focussing attention on the slow and long wavelength hydromodes $\omega \to 0$, $q \to 0$ monitoring BIM demixing, one can safely restrict Eq. (4) to its static limit $\omega \to 0$

$$S = \frac{8\pi}{3}\left(Z_p e^2\right)^2 \beta V_p \int_0^\infty dq S_{zz}(q) \qquad (6)$$

in terms of $S_{zz}(q) = \int_0^\infty d\omega S_{zz}(q,\omega)$. Eq. (6) also highlights the expected LVISD linear

V_p – dependence $\leq \overline{V_{thi}}$. Eq. (6) implies an average over every ω-fluctuation, available to $S_{zz}(\vec{q},\omega)$.

Critical S_{zz} (q)

Mean field classical description of BIM demixing could be rather straightforwardly explained with the static charge-charge structure factor

$$S_{ZZ} = \frac{\Sigma|t|^{-\gamma}(qa_i)^2}{3\overline{\Gamma}\overline{Z}^2\left((q\xi)^2+1\right)} \qquad (7)$$

where $t = \frac{T - T_c}{T_c}$, T_c = critical temperature, $\gamma = 1$ and ξ = ion-ion correlation length featuring $\lim_{|t|\to 0} \xi \to \infty$.

$\overline{Z} = C_1Z_1 + C_2Z_2$ and $\overline{\Gamma} = C_1\Gamma_1 + C_2\Gamma_2$.

$\sum$ denotes a constant normalizing factor accessed through the sum rule (q in $\overline{a_i}^{-1}$)

(where $\overline{a_i} = C_1a_1 + C_2a_2$)

$$\int_0^\infty dqq^2\left[S_{zz}(q) - \overline{z^2}\right] = -\frac{3\pi}{2}, \qquad (8)$$

where $\overline{z^2} = 1 + C_1C_2(Z_1 - Z_2)^2/\overline{Z}^2$.

Expression (7) mostly emphasizes long distance hydromodes, of significance at critical demixtion.

Paying a first attention to nonpolarizable BIM with a fixed and rigid electron background, the correlation length reads as

$$\left(\frac{\bar{a}_i}{\xi}\right)^2 = 3\bar{\Gamma}\bar{z}^{-2}\frac{D_I}{D_R} \quad , \qquad (9)$$

where D_I and D_R respectively denote the $q \to 0$ limit of

$$D_1(q) = \bar{Z}^2 - C_1C_2\left[Z_1^2\hat{C}_{22}^R(q) + Z_2^2\hat{C}_{11}^R(q) - 2Z_1Z_2\hat{C}_{22}^R(q)\right] \quad , \qquad (10)$$

and $$D_R(q) = 1 - c_1\hat{C}_{11}^R(q) - c_2\hat{C}_{22}^R(q) - c_1c_2\det\left|\hat{C}_{\alpha\beta}^R(q)\right| \quad , \qquad (11)$$

in terms of

$$\hat{C}_{\alpha\beta}^R(q) = \hat{C}_{\alpha\beta}(q) + Z_\alpha Z_\beta\hat{v}(q) \quad , \qquad (12)$$

$\hat{C}_{\alpha\beta}^R(q)$ denotes the partial direct correlation function, viewed in the (OZ) equations

$$\hat{h}_{\alpha\beta}(k) = \hat{C}_{\alpha\beta}(q) + \sum_{\nu=1}^{2} c_\nu\hat{h}_{a\nu}(q)\hat{C}_{\nu\beta}(q) \quad , \qquad (13)$$

The right hand side of Eq. (12) also features the dimensionless and screened Coulomb potential

$$\hat{v}(q) = \frac{4\pi\beta e^2\bar{n}_i}{k^2\varepsilon(q)} \equiv \frac{3\bar{\Gamma}}{\bar{a}_i^2}\frac{1}{k^2\varepsilon(q)} \quad , \qquad (14)$$

with the dimensionless static electron fluid dielectric function $\varepsilon(q)$. Close to criticality, one expects a characteristic diverging behavior of the correlation length, so that

$$\xi = \xi_0^{\pm}|t|^{-\nu} \quad , \quad t \to 0 \qquad (15)$$

with $\nu = 0.5$, in a standard mean field OZ approximation.

Superelastic LVISD

The introduction of expression (7) into Eq. (6), thus yields for $q\bar{a}_i \le 1$,

$$S = \frac{8\pi}{3}\left(Z_p e^2\right)^2 \cdot \frac{\beta V_p}{\bar{a}_i} \cdot \frac{\Sigma|t|^{-1}}{\overline{\Gamma Z}^2}\left(\frac{\xi}{\bar{a}_i}\right)^2 \cdot \left[1 - \mathrm{Tan}^{-1}\left(\frac{\xi}{\bar{a}_i}\right)\right] , \qquad (16)$$

demonstrating that ξ-diverging behavior (Eq.15) is compensated by that in Eq. (7).

Now we pay attention to correlation length (Eq. (9)) estimates by solving simultaneously OZ equs. (13) with (HNC) equations

$$g_{\alpha\beta}(r) = \exp\left[h_{\alpha\beta}(r) - (C^R_{\alpha\beta}(r)\right] , \qquad (17)$$

valid for any Γ_i values.

Lindhard screening involves (cf Fig. 1)

$$\varepsilon(k) = \frac{k^2 + k_{TF}^2 g_L(x)}{k^2} , \qquad (18)$$

where $k_{TF} = \left(6\pi n_e e^2 / E_F\right)^{1/2}$ denotes the Thomas-Fermi wave vector and the function $g_L(x)$ depends only on the dimensionless variable $x = k/2k_F$, with

$$g_L(x) = \frac{1}{2} + \frac{1-x^2}{4x}\ell n\left|\frac{1+x}{1-x}\right| , \qquad (19)$$

and $k_F = (3\pi^2 n_e)^{1/3}$, Fermi wave number in terms of electron density n_e, while $E_F = \hbar_F^2 k_F^2 / 2m_e$.

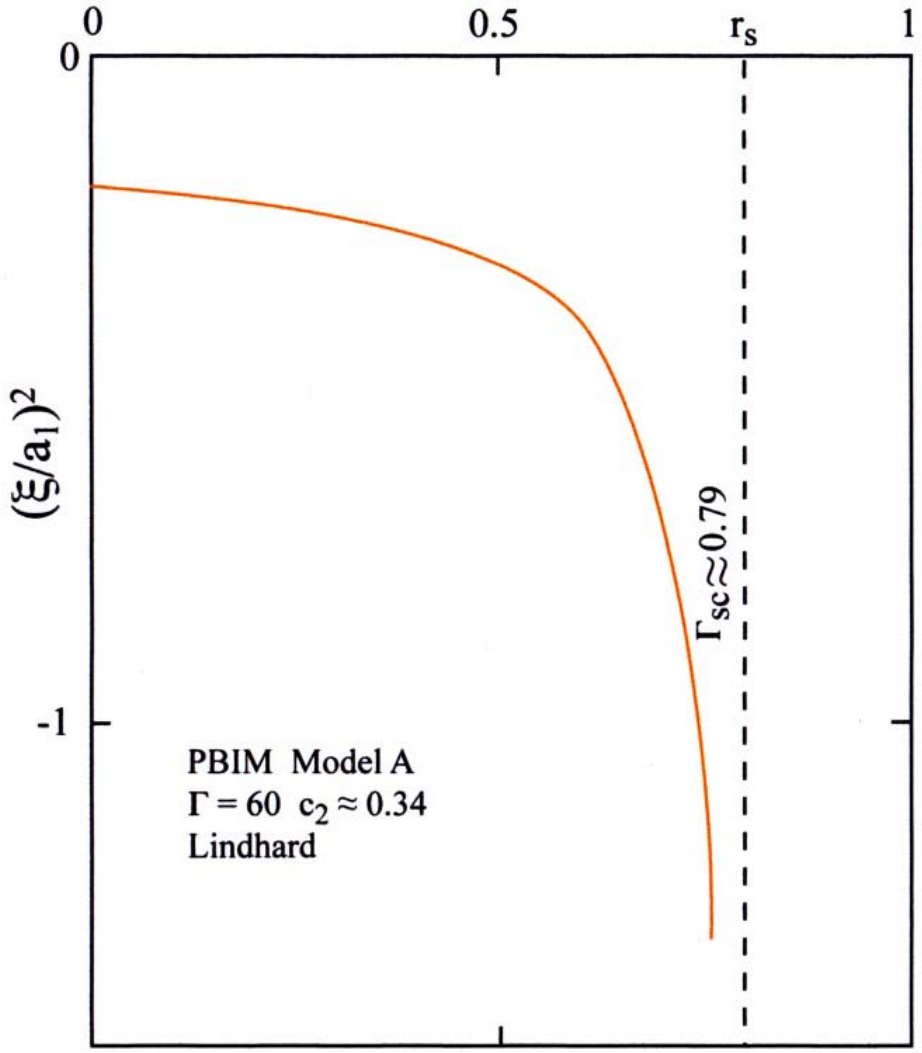

FIG. 1- Plot of the reduced squared correlation length $(\xi/a_1)^2$ in terms of r_s along a critical and vertical line (34% He, $\Gamma = 60$) with Lindhard screening. There ξ^2 remains negative.

$$g(x) = \frac{g_L(x)}{1 - \frac{k_{TF}^2}{k^2} g_L(x) G(x)} , \qquad (20)$$

where $G(x) = \frac{x^2}{2x^2 + 1/2}$, includes exchange-correlation contributions into the jellium background.

Present critical conditions are now significantly different. On Fig. 2, critical demixtion occurs at C_2=0.75 in lieu of C_2=0.34 on Fig. 1 for same $\Gamma = 60$. More importantly, ξ^2 is now allowed to increase positive on the largest r_s range side.

The resulting correlation length is now raising strongly when $|t| \rightarrow 0$, up to the standard mean field behavior $(\xi/a_1)^2 >> 1$.

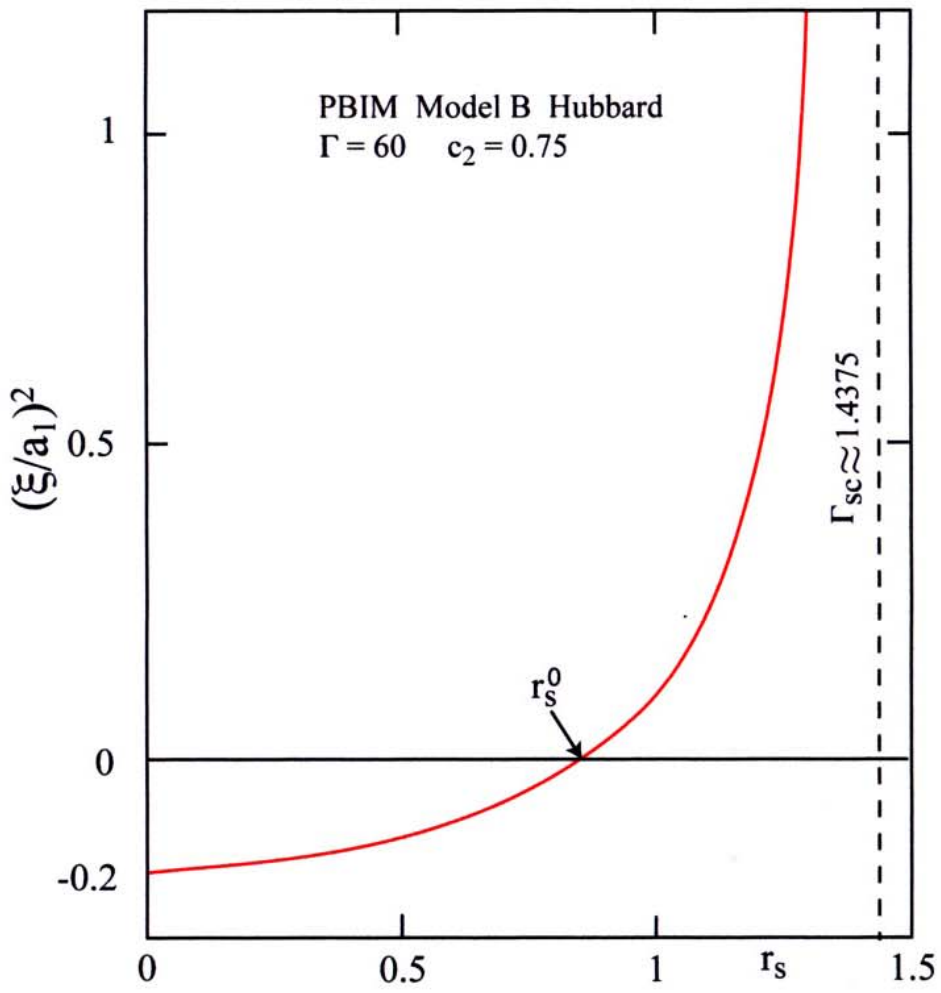

Fig. 2- PBIM model B with Hubbard screening. Plot of the reduced squared correlation length $(\xi/a_1)^2$ as a function of r_s along a critical and vertical line (75% He at $\Gamma = 60$) ξ^2 is now allowed to change sign for $r_s \geq r_s^0$.

The given LVISD is now negative featuring a superelastic interaction between the low velocity incoming ion projectile and the PBIMB target.

It can also be appreciated that before turning negative, LVISD (16) vanishes for $(\xi/a_1)^2 \sim 1.65$. The prefactor $\sum$ in Eq. (16) is then straightforwardly derived from the sum rule (8) under the alternative forms,

$$\Sigma = \left(-\frac{3\pi}{2} + \overline{z^2}\right)^3 \frac{D_R|t|}{D_I} \tag{21a}$$

in terms of BIM thermodynamics and also (cf. Eq. (15))

$$\Sigma = q\overline{\Gamma}^2 \overline{z^2}\left(-\frac{3\pi}{2} + \overline{z^2}\right)^3 \left(\frac{\xi_0^{\pm}}{\bar{a}_i}\right) \tag{22b}$$

The present developments highlight for the first time the intriguing interplay of a first order demixing process in a strongly coupled and binary ionic mixture with a low velocity incoming ion beam. The latter may be envisioned for diagnostics purposes or target conditioning in the subfields of ICF and warm dense matter, for instance.

Within a fundamental statistical physics perspective, it should be appreciated that the above results document unambiguously the potentialities of probing collective very long wavelength phenomena occuring in a plasma target with low velocity ion beams via the evaluation of a transport coefficient, featured in the present context by a stopping power mechanism.